Main Text

Functionalizing DNA Origami by Triplex-Directed Site-Specific Photo-Crosslinking

Shantam Kalra,[1$] Amber Donnelly,[1$] Nishtha Singh,[1$] Daniel Matthews,[1] Rafael del Villar-Guerra,[1**] Victoria Bemmer,[2] Cyril Dominguez,[1] Natalie Allcock,[3] Dmitry Cherny,[1] Andrey Revyakin,[1*%] and David A. Rusling[4*]

[1]Department of Molecular and Cell Biology and Leicester Institute of Chemical Biology, University of Leicester, Henry Wellcome Building, Lancaster Road, LE1 7RH, UK.
[2]Centre for Enzyme Innovation, School of Biological Sciences, Institute of Biological and Biomedical Sciences, University of Portsmouth, Portsmouth PO1 2DY UK.
[3]Core Biotechnology Services Electron Microscopy Facility, University of Leicester, Hodgkin Building, Lancaster Road, Leicester, LE1 7RH, UK.
[4]School of Pharmacy and Biomedical Sciences, University of Portsmouth, St. Michael's Building, White Swan Road, Portsmouth, Hampshire, PO1 2DT, UK.
[$]Equal contribution
**Present address: Biopharmaceuticals Development, R&D, AstraZeneca, Cambridge, UK.
[%]Present address: Max Planck Institute of Immunobiology and Epigenetics, Stübeweg 51, D-79108 Freiburg, Germany
*Corresponding authors: revyakin@ie-freiburg.mpg.de, david.rusling@port.ac.uk

ABSTRACT

Here we present a universal method to introduce functionality and improve the structural integrity of DNA origami in a one-pot reaction. Our strategy involves adding nucleotide sequences to adjacent staple strands so that, upon origami assembly, the add-on sequences form short hairpin duplexes targetable by psoralen-labelled triplex-forming oligonucleotides (pso-TFOs) bearing other functionality. Subsequent irradiation with UVA light generates psoralen adducts with one or both hairpin staples leading to site-specific attachment of the pso-TFO to the origami with >80% efficiency. Bis-adduct formation between strands in proximal hairpins further tethers the TFO to the structure and generates 'super-staples' that improve the structural integrity of the complex. We also show that crosslinking reduces the sensitivity of the functionalized origami to thermal denaturation and disassembly by T7 RNA polymerase. Our strategy is scalable and cost-effective as it works with existing DNA origami structures, does not require scaffold redesign, and can be achieved with just one psoralen-modified oligonucleotide. It is also non-damaging to the origami scaffold, as well as to introduced fluorescent functionalities.

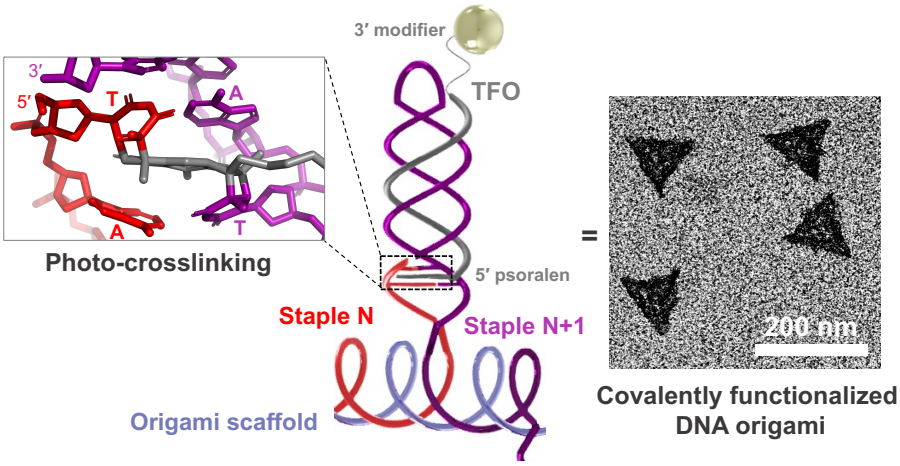

Table of contents graphic.

INTRODUCTION

Nucleic acid (NA) nanotechnology is a bottom-up nanofabrication approach that harnesses the self-assembly properties and well-understood structure of nucleic acids to create molecular objects or patterns ranging from a few nanometres to a few microns in characteristic size.[1] DNA origami is a subfield of NA nanotechnology in which a long single-stranded DNA "scaffold" strand is woven in two or three dimensions using a few hundred shorter DNA "staple" strands.[2-3] DNA origami are straightforward to design,[4] relatively cost-effective to produce, and offer potential applications in a wide range of disciplines.[5] Examples of applications of DNA origami in biomedicine include vaccines,[6] enzymatic cascades,[7] biological nanosensors,[8] nanorobotics,[9] drug delivery,[10] super-resolution microscopy,[11] structural biology,[12] basic single-molecule research,[13] and many others.

Although origami have been functionalized with numerous types of organic and inorganic moieties, methods that allow their site-specific attachment to the structure are still not trivial.[5] Such guest molecules are frequently conjugated to oligonucleotides that are introduced before or during the assembly of the nanostructure. However, some molecules cannot tolerate the relatively harsh conditions required for origami folding, *e.g.,* if the guest molecule is a protein, high annealing temperatures can lead to its denaturation. Moreover, the attachment of more than one guest molecule to the structure requires its conjugation to individual staples which can substantially increase cost. A different approach relies on the recruitment of conjugated oligonucleotides *via* Watson-Crick (W-C) hybridisation to single-stranded staple overhangs projected from the assembled nanostructure. However, such non-covalent interactions can result in stochastic dissociation of the oligonucleotides and loss of the introduced component. Other post-assembly modification strategies exist, such as the recruitment of cargo to specific sequences or reactive groups introduced into the structure.[14,15,16] However, these strategies are not generally applicable as they first require attaching the guest molecule to a specific targeting agent, *e.g.,* aptamers, streptavidin, or zinc finger proteins.[17,18]

Once assembled, functionalized origami suffer from several other limitations that have restricted their widespread use.[19] First, origami are not covalently sealed; rather, they are held together by weak (W-C) hydrogen bonding between the single-stranded DNA scaffold and hundreds of staples. This makes the nanostructures sensitive to thermal denaturation,[20] chaotropic agents,[21] depletion of metal ions,[22] changes in pH,[23] and other treatments. Second, the duplex regions of origami are susceptible to degradation by DNA processing enzymes found in biological media and live cells (*e.g.,* nucleases,[24] RNA polymerase,[25] *etc.*). In these cases, this can lead to the loss of guest molecules held in place by the relatively short staple

oligonucleotides assembled within the structure. Various methods have been developed to improve the stability of duplex regions within DNA origami, such as through the enzymatic[26] or chemical ligation[27,28] of nick sites located between adjacent staple strands, or the "welding" of strands within or projected from the origami by high-energy ultraviolet light.[29,30,20] However, these approaches are not always cost-effective and can compromise the application of introduced functionalities, *e.g.,* due to photobleaching of incorporated fluorophores (D. Mathews, A. Revyakin, unpublished).[31] Most importantly, none of these strategies have been coupled with the functionalisation process.

Here we present a novel strategy based on triplex-directed photo-crosslinking that can be used to introduce functionality *and* improve the structural integrity of DNA origami in a single one-pot reaction (**Fig 1**). Triplex-forming oligonucleotides (TFOs) are sequence-specific DNA recognition agents[32,33] that bind within the major groove of polypurine-polypyrimidine duplex sequences.[34] TFOs have been used as a means to attach functional groups to DNA by the conjugation of non-nucleic acid components to the 5′ or 3′ ends of the oligonucleotide (*e.g.* fluorescent dyes, reactive groups, proteins, *etc.*).[34,35] The site-specific incorporation of the attached functional group is achieved by targeting the TFO to appropriate polypurine-polypyrimidine sites embedded within the DNA sequence.[36,37,38] TFOs have also been used to direct site-specific crosslinking reactions within DNA by attaching the photo-crosslinking agent 4,5,8-trimethylpsoralen (psoralen) to the 5′ end of the oligonucleotide.[39,40,41] TFO binding directs psoralen intercalation at a TpA step flanking the 5′-end of the triplex-duplex junction. Subsequent irradiation at 365 nm leads to a 2+2 cycloaddition reaction between the psoralen and opposing thymidine residues, crosslinking the two duplex strands and the oligonucleotide to the DNA. Our strategy harnesses both the functionalisation and crosslinking properties of TFOs to site-specifically modify DNA origami. Moreover, through appropriate design, we show that this approach can be used to reduce the sensitivity of the functionalised origami to thermal denaturation and to disassembly by T7 RNA polymerase. Our strategy is cost-effective as it works with existing DNA origami structures, does not require scaffold redesign, and can be achieved with a single psoralen-modified oligonucleotide. The crosslinking reaction is fast (seconds) and is therefore scalable, energy-efficient, and non-damaging to the structural integrity of the origami scaffold, as well as to fluorescent functionalities introduced into the structure.

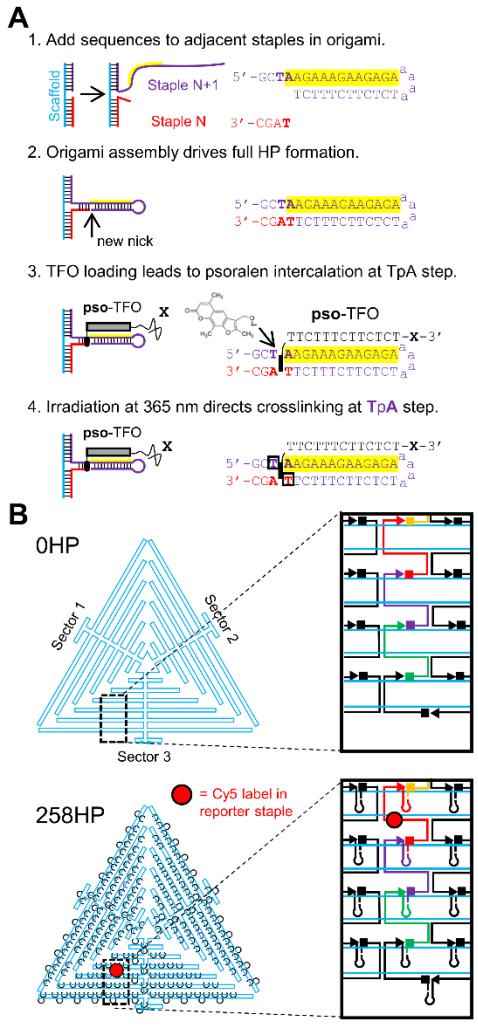

Figure 1. Targeting, crosslinking and functionalization of DNA origami by psoralen-modified TFOs: (A) Targetable hairpins are introduced into origami by the attachment of nucleotide sequences to the 5′ and 3′ ends of any two adjacent staples (*i.e.,* staple N and N+1). The extension of staple N+1 (purple) encodes for a stem-loop hairpin and contains the TFO binding sequence (shown in yellow) and a 4-nt linker that contains the TpA sequence destined for psoralen crosslinking (in bold). Staple N (red) encodes the 4-nt compliment to the linker so that, upon origami assembly, a crosslinkable duplex between adjacent hairpins is formed. Targeting by a pso-TFO leads to psoralen intercalation across the TpA step (shown as a black bar). Irradiation with UVA (365 nm) light triggers mono- and bis-adduct formation between psoralen and the thymidine bases in the TpA step (shown by the boxes), covalently attaching the TFO to the origami. Bis-adduct formation between staples in proximal hairpins further tethers the TFO and leads to formation of “super-staples” that enhance the structural integrity of the origami. Functionalization is achieved using pso-TFOs that carry additional moieties (X) at their 3′ end; **(B)** Design of the prototypical DNA origami triangle used in this study. Scaffold routing for 0HP and 258HP origami are shown in blue and the 258 hairpins in 258HP are shown as black semi-circles. Routing of the staples ensured that staple-staple junctions and TFO-binding hairpins alternated between opposite faces of the triangle to allow functionalization of origami on both sides. The folding, crosslinking and degradation of these complexes was monitored using a Cy5-labelled reporter staple 1 (shown in red). Adjacent to staple 1 are reporter staples 0, 2, and 3 (orange, purple, and green, respectively) which are used to illustrate how TFO-binding hairpins are formed by adjacent staples.

RESULTS

Design of targetable hairpin-modified origami

Due to sequence binding constraints and a requirement for a TpA step for crosslinking, it is not possible to use pso-TFOs to target origami folded from commercially available scaffolds directly, *e.g.,* M13mp18 or its derivatives.[42] Our strategy therefore involved introducing a crosslinkable TFO target duplex sequence into the stem-loop hairpin(s) (HP) projected from the origami staples. This was achieved by extending the 3′ end of a specific origami staple(s) with a 32-nt sequence that folds intramolecularly into a 12-nt HP separated from the scaffold *via* a 4-nt single-stranded linker sequence (shown in purple in **Fig 1A**). The HP encodes an appropriate TFO-binding sequence, and the single-stranded linker encodes the "top" strand of the TpA duplex sequence destined for psoralen crosslinking. It also required extending the 5′ end of the adjacent staple(s) with a single-stranded 4-nt sequence which encodes the complementary "bottom" strand of the TpA sequence (shown in red in **Fig 1A**). Upon origami assembly, the 3′ linker sequence from one staple (Staple N+1) is positioned next to the 5′ linker complement from the adjacent staple (Staple N), generating a TpA duplex that can be crosslinked between thymidine residues positioned by the neighbouring staple strands. Crosslinking of multiple adjacent HPs was expected to form "super-staples" that further tether the TFO to the structure and increase the structural integrity of the origami. Functionalization is made possible by the attachment of cargo to the free 3′-end of the pso-TFO (shown as X in **Fig 1A**).[40]

To test our strategy, we designed[4] a prototypical origami triangle[3] held together by 261 staples and comprised of three independently folding sectors (**Fig 1B**). We extended both the 3′ and 5′ ends of 258 staple strands with the sequences described above and positioned hairpins on either side of the origami. We folded the 258HP nanostructure (258HP) using a 8064-nt M13 single-stranded DNA scaffold[42] and a 3-fold molar excess of HP-staples (**Fig 1B**). As a control, we also folded hairpin-free triangles (0HP) which were identical in staple routing but contained no hairpins. Agarose gel electrophoresis (AGE) of folded 0HP and 258HP origami revealed bands consistent with the successful formation of both types of nanostructures (**Fig S1**). As expected, the mobility of 258HP was reduced compared to 0HP, consistent with the extra molecular mass of 258 hairpins (mobility at ~3.0 kb versus ~2.5 kb, respectively). Subsequent imaging of purified[43] nanostructures by transmission electron microscopy (TEM) revealed that the 258HP origami formed homogeneous particles of the desired size and shape (**Fig 2A, Top**). In contrast, imaging of the 0HP nanostructures revealed that these hairpin-free triangles tended to appear warped (**Fig 2A, Bottom**), indicating that they might be flexible in

solution.[44] Taken together, these results show that addition of hairpins at the staple-staple junctions is compatible with origami folding and might also rigidify the nanostructure.

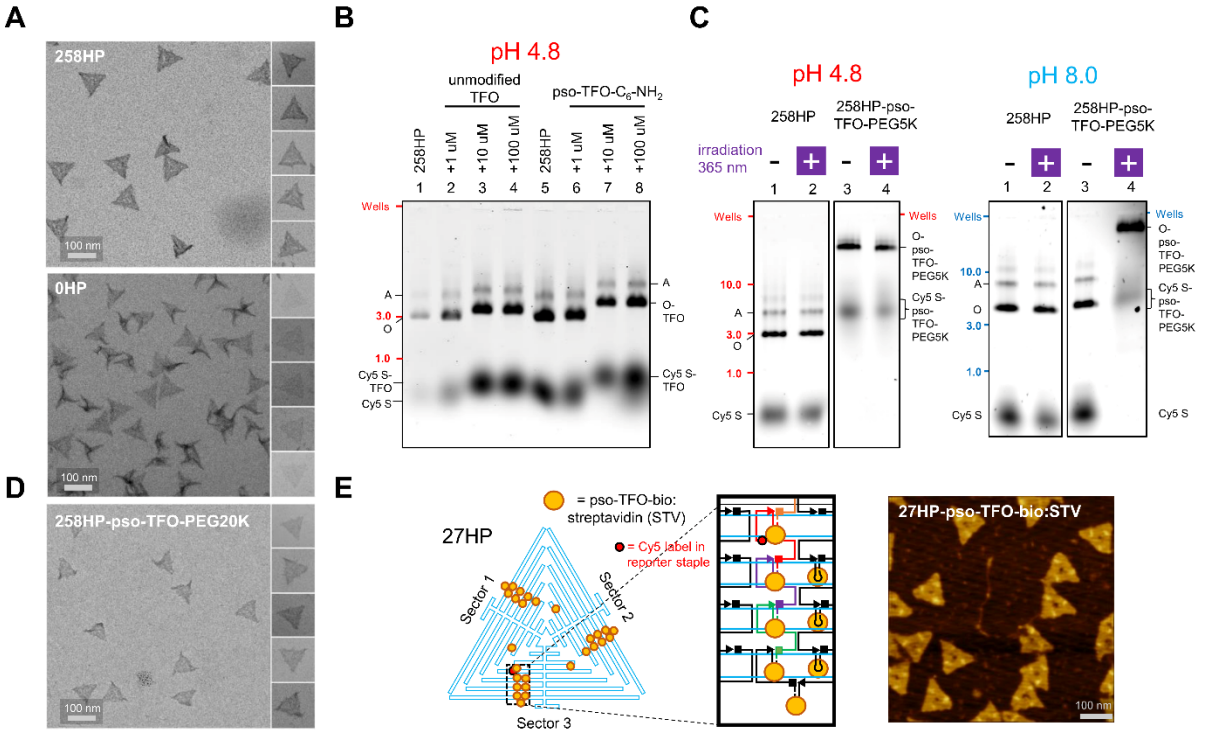

Figure 2. Targeting of origami hairpins by TFOs bearing additional moieties. (A) Representative TEM images of purified 258HP (top image) and 0HP (bottom image) origami triangles; **(B)** AGE analysis of the raw folding mix of 258HP origami loaded at different concentrations of TFOs. Origami were first prepared by annealing 50 nM scaffold with 150 nM staples. The TFOs were then supplied at the stated concentrations and the reaction incubated at pH 4.8 for 1 hr at room temperature. Bands corresponding to the origami and the free staples were visualized by scanning for Cy5-labeled staple 1 fluorescence. A DNA ladder was visualized by scanning for ethidium bromide fluorescence and positions of the 1, 3 and 10 kb bands are as indicated. Lanes 2-4 contained samples incubated with the unmodified TFO, whilst lanes 6-8 contained the dual-labelled pso-TFO-C6-NH_2. “O” – origami monomer; “A” – origami aggregate/oligomer (expected to form during origami foldingd[43]); “O-TFO” – origami loaded with TFO, “S” – Cy5-labeled staple 1, “S-TFO” – staple 1 loaded with TFO; **(C)** Functionalization and crosslinking of 258HP origamis: effects of pso-TFO-PEG5K and 365 nm irradiation on the mobility of 258HP in AGE at different pH. One-pot assembly conditions were used to prepare 258HP loaded with pso-TFO-PEG5K. The samples were then irradiated with 365 nm light and analysed by AGE at pH 4.8 (left gel, annotated in red) and pH 8.0 (right gel, annotated in blue). Bands corresponding to the origami and the free staples were visualized by scanning for Cy5-labeled staple 1 fluorescence. Positions of the wells in the gel and the 1-, 3-, and 10-kb DNA ladder bands are as indicated. Labels of nucleic acid species are as in B; **(D)** Representative TEM images of one-pot crosslinked and purified 258HP origami loaded with pso-TFO-PEG20K; **(E)** Site-specific targeting of 27HP origamis with pso-TFO-PEG_4-biotin. *Left:* scaffold routing for 27HP origami which contains 27 TFO-binding hairpins in three clusters. TFO-bound streptavidin molecules are shown as orange circles. *Right:* One-pot assembly conditions were used to prepare 27HP origami loaded and crosslinked with pso-TFO-PEG_4-biotin. The complexes were then incubated with 100 μM streptavidin for 30 min, dried and imaged by AFM.

HP-origami are targetable by unmodified and modified pso-TFOs

We next investigated if the hairpins in the 258HP origami could be loaded with a TFO by incubating the raw folding mixtures with progressively increasing concentrations of an unmodified 13-nt TFO. Loading and AGE analysis were performed at pH 4.8 to drive the formation of C^+-GC Hoogsteen bonds in the TFO-hairpin complexes (**Fig 2B**). Significant upward shifts in mobility for the origami and for the free HP staples were observed at [TFO]=10 μM and [TFO]=100 μM, indicating TFO binding (compare lanes 1, 3 and 4), whilst no significant shift was observed at the lower [TFO] = 1 μM (lane 2). We then repeated the AGE experiment using a dual-labelled TFO carrying psoralen at its 5′ end and a C6-NH_2 group at its 3′ end (pso-TFO-C6-NH_2) (**Fig 2B**). We again observed upward shifts in the mobility of the nanostructure and free HP-staples at the same concentrations seen with the unmodified TFO (compare lanes 5, 7, and 8). The shift of the origami by TFO-C6-NH_2 was more pronounced compared to the effect of unmodified TFO on account of the higher molecular mass and charge of the 5′ and 3′ modifications on TFO. These results indicate that HP-bearing origami are targetable with both unmodified and modified TFOs.

We next sought to streamline the preparation of TFO-loaded origami by combining origami folding with TFO loading in a simple one-pot reaction. To quantify TFO loading, we used a TFO labelled with Alexa Fluor 647 at the 3′ end of the oligonucleotide (TFO-A647). Experiments were undertaken using a TFO concentration of 100 μM, *i.e.*, ~7-fold excess of TFO to individual hairpins in origami (**Fig S2)**. We first attempted the one-pot assembly at pH 4.8 (*i.e.,* under conditions that favour TFO binding), but AGE analysis revealed poor folding of the 258HP origami structure (lane 4, **Fig S2A**). The same was observed for folding at pH 4.8 in the absence of TFO, indicating that it was the low pH and not the TFO that interfered with folding (lane 3, **Fig S2A**).[45] We then repeated the folding at pH 8.0 (*i.e.*, under conditions that favour origami annealing) and characterised complex formation by AGE analysis at pH 4.8. This revealed robust folding and labelling of the 258HP origami and free HP staples by TFO-A647 (compare lanes 5 and 6, **Fig S2A**). This finding was initially counter-intuitive, since C^+-GC Hoogsteen bonds are disfavoured at this pH.[34] However, we explain this result by the mass action of the concentrated TFO in the folding reaction. Strikingly, ultracentrifugation of the 258HP-TFO-A647 folding mixture at pH 4.8 revealed a distinct blue band (visible with the naked eye) at the expected location of the origami in the glycerol gradient (**Fig S2B**). Further estimation of Alexa Fluor 647 fluorescence in the purified fraction revealed ~90% loading of the 258 hairpins with TFO-A647 (**Fig S2C**). We conclude that, under appropriate annealing conditions, HP-containing origami can be folded and loaded with TFO in a single step.

We then asked if one-pot assembly can be used to prepare origami targeted with TFOs modified with bigger functional groups. To test this, we used pso-TFOs modified at their 3′ ends with poly (ethylene glycol) moieties of molecular weights 5,000 and 20,000 (pso-TFO-PEG5K and pso-TFO-PEG20K, respectively). Such PEG modifications might protect origami from non-specific protein binding.[46,47] As before, we annealed the complexes at pH 8.0 in the presence of an excess of pso-TFO-PEG5K/20K and assayed the formation of the origami-TFO complex by AGE at pH 4.8. Analysis of the gels revealed that the attachment of multiple PEG groups to the nanostructures severely reduced the mobility of the origami complexes (**Fig S3A, top and Fig S3B**). To verify that 258HP-pso-TFO-PEG complex formation was through TFO-HP Hoogsteen interactions, we also performed AGE analysis of the pso-TFO-PEG5K complex at pH 8.0, with the expectation that increasing the pH during electrophoresis would lead to dissociation of the pegylated TFO. As expected, the mobility of the nanostructure at pH 8.0 returned to that observed for the TFO-free 258HP nanostructure (**Fig S3A, bottom**). These results are consistent with formation of unstable 258HP-pso-TFO-PEG5K/20K complexes, with the PEG coats held in place by the weak Hoogsteen hydrogen bonds.

We next sought to stabilise the origami-TFO-PEG complexes through directed photo-crosslinking using the psoralen functionality on the 5′ end of the TFO. It was expected that irradiation at 365 nm would induce formation of either mono- or bis-adducts between the pso-TFO and the hairpin staples. To test this, we folded the 258HP-pso-TFO-PEG5K origami in one-pot reaction and irradiated the complex using a home-built light-emitting diode (LED) setup (**Fig S3C**). The stability of the crosslinked origami-TFO complexes was again determined by AGE at different pH (**Fig 2C**). AGE analysis at pH 4.8 revealed that, as intended, the 258HP loaded with pso-TFO-PEG5K retained their reduced mobility after crosslinking (**Fig 2C, left gel**). In contrast, AGE analysis at pH 8.0 revealed that only irradiated origami-TFO complexes retained a reduced mobility, whilst the mobility of the non-irradiated complex returned to that observed with TFO-free 258HP (**Fig 2C, right gel**). Further TEM imaging of the purified crosslinked PEGylated complexes revealed homogeneous origami particles that appeared essentially identical to the TFO-free 258HP nanostructures, presumably due to the low contrast of the PEG moieties (**Fig 2D**). We conclude that TFOs can deliver diverse functional groups onto origami, and that psoralen crosslinking can be used to covalently attach the group to the DNA.

Since TEM imaging of the PEG-coated origami revealed structures essentially identical to the hairpin-only origami, we sought an independent verification of the site-specific targeting of the hairpins by TFOs. For these experiments we used triangles that contained 27 hairpins grouped into three clusters of nine adjacent hairpins, with one cluster per triangle sector (27HP, **Fig**

S4). To target these hairpins, we used a pso-TFO labelled with a biotin group at the 3′ end of the oligonucleotide (pso-TFO-bio), which enabled the recruitment of streptavidin tetramers (STV) to the bound oligonucleotides. The 27HP-pso-TFO-bio origami complex was folded, purified, irradiated, and incubated with STV for 1 hr. AGE analysis at pH 8.0 revealed that the complexes were progressively shifted by STV, with apparent saturation achieved at a ratio of ~10:1 STV to hairpins in origami (**Fig S5A**). No STV-induced shift was observed for TFO-free 27HP (**Fig S5B**). Quantification of fluorescence of saturated 27HP-pso-TFO-bio:STV complexes stained with a biotin-Alexa647 conjugate revealed a ~26.7:1 ratio of origami backbone to streptavidin, consistent with the theoretical 27:1 ratio (**Fig S5A** and data not shown). TEM imaging of 27HP-pso-TFO-bio:STV complexes did not provide sufficient contrast to reveal locations of STV-loaded hairpins (data not shown). In contrast, AFM imaging of the STV-saturated 27HP-pso-TFO-bio origami revealed, as expected, triangles featuring “blobs” in three clusters at the expected locations of all three sectors (**Fig 2F**).[48] AFM images of 0HP structures incubated with the saturating concentration of STV, and AFM images of 27HP-pso-TFO-bio complexes obtained without STV, revealed no such clusters (**Fig S5C**). We conclude that TFOs can accurately target specific sites in HP-containing DNA origami, and that the number and positioning of introduced groups can be varied through HP incorporation.

Mechanism and specificity of TFO-directed photo-crosslinking

Since irradiation of pso-TFO-loaded origami with 365 nm light stabilized the interactions between pso-TFO-PEG/bio and HP-origami, we sought further insight into the mechanism of this stabilization. To this end, we designed a further DNA origami containing exactly one hairpin (1HP) (**Fig S4** and **Fig 3A**). In this origami, the hairpin is formed between a reporter staple labelled with Cy5 (staple 1, shown in red) and an adjacent staple (staple 0, shown in orange). It was expected that irradiation of 1HP origami loaded with pso-TFO would result in the formation of mono- and bis-adducts between the 13-mer pso-TFO and these two staples. These adducts would then be detectable by denaturing polyacrylamide gel electrophoresis (PAGE) as an upward shift in mobility of the fluorescent staple 1. To minimize the ambiguity in identifying crosslinking products, we also created a minimal three-way construct (1HP-junction) (**Fig 3A**). 1HP-junction contains the same hairpin formed by staples 0 and 1 but uses a short “pseudo-scaffold” to mimic the scaffold in the 1HP origami. If the mechanisms of pso-TFO-driven crosslinking within the minimal 1HP junction and the full 1HP origami were the same, we would expect to observe identical patterns of Cy5-labeled adducts in PAGE analysis of both irradiated constructs.

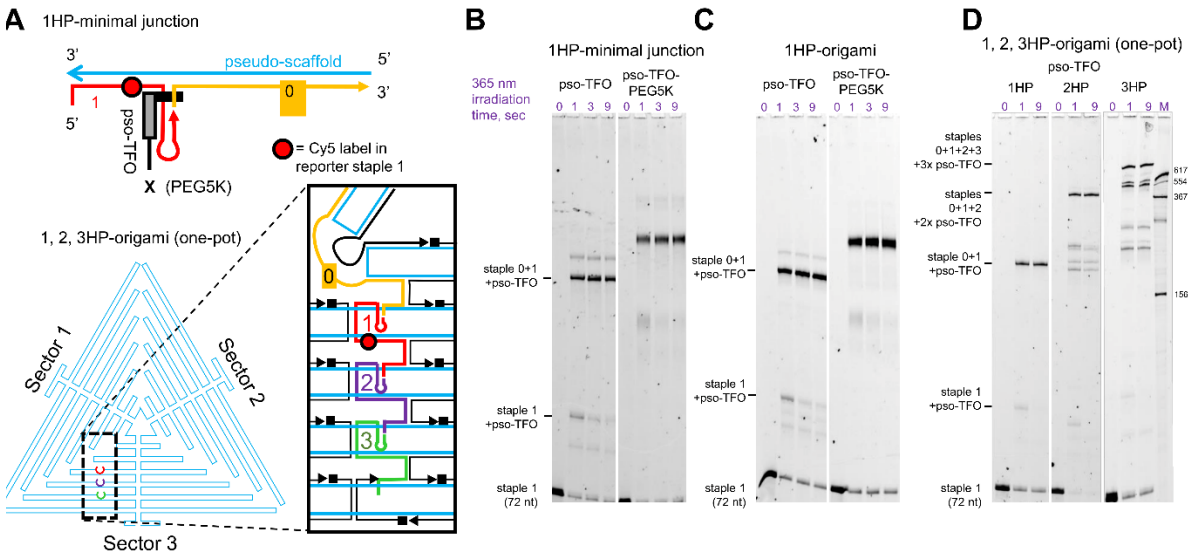

Figure 3. Mechanism and specificity of pso-TFO-driven crosslinking. (A) Experiments were undertaken on 1, 2, 3HP origami containing 1, 2, or 3 TFO-binding hairpins, respectively. HP1 was assembled using 3′-hairpin-modified staples 0 and 1, HP2 – using 3′-hairpin-modified staples 0, 1 and 2, and HP3 – using 3′-hairpin-modified staples 0, 1, 2, and 3. As a control, a 1HP minimal junction (top) was assembled from staples 0 and 1 but used a minimal "pseudo-scaffold" oligo in place of origami scaffold. Each of these complexes contained staple 0 (orange) which lacked the 3′-hairpin extension. They also contained Cy5-labelled staple 1 (red) which allowed the products of the crosslinking reaction to be monitored; **(B-C)** Experiments undertaken on 1HP-minimal junction and 1HP origami that were first folded and then saturated with either the pso-TFO or its PEG5K conjugate. Samples were subjected to irradiation at 365 nm for the time points shown, and the products of the reaction were denatured and then separated on an 8% denaturing PAGE gel. Bands were visualized by scanning for Cy5-labeled staple 1 fluorescence. (**D**) Experiments undertaken on 1HP, 2HP and 3HP origami that were prepared by one-pot annealing in the presence of either pso-TFO or its PEG5K conjugate. They were subjected to irradiation at 365 nm for the time points shown, and the products of the reaction were denatured and then separated on an 8% denaturing PAGE gel. Lane M contains Cy5-labeled amplified PCR products of indicated lengths, denatured and separated on the same gel.

We first folded the minimal 1HP-junction and loaded it with an excess of pso-TFO. We then irradiated the complexes with the LED for 1, 3, and 9 seconds and separated the products using PAGE (**Fig 3B**). Analysis of the gel revealed that, after 1 second of irradiation, ~89% of the Cy5-labelled staple 1 was converted into products of higher molecular weight. The main product contained ~60% of signal and was consistent with the formation of a bis-adduct comprised of staple 0, staple 1 and the TFO.[40,41] An additional product of intermediate molecular weight that contained 19% of the signal likely corresponded to the mono-adduct formed between the Cy5-labelled staple 1 and the TFO. To support this, it was observed that the proportion of the mono-adduct decreased by ~7% upon irradiation for 9 seconds, while the proportion of the bis-adduct increased by ~8%. In addition, both products migrated slower when pso-TFO-PEG5K was used in place of the pso-TFO. Overall, these results indicate that the 1HP-junction loaded with pso-TFO gets rapidly and specifically crosslinked upon

irradiation, with formation of a bis-adduct containing pso-TFO and the two hairpin-forming staples.

We then asked if 1HP origami is crosslinked by a mechanism like the minimal 1 HP junction. We found that, for the 1HP origami-pso-TFO complex, the patterns of the Cy5-labeled products, their mobilities, and the kinetics of their formation were essentially indistinguishable from those in the minimal 1HP junction-pso-TFO complex (**Fig 3C**). The observed efficiencies of the bis-adduct formation increased for irradiation times of 1, 3, and 9 seconds (74%, 80% and 81%, respectively), while the efficiencies of the intermediate mono-adduct formation decreased for the same time points (10%, 4%, and 3%, respectively). The same crosslinking patterns and kinetics were observed when we repeated the 1HP origami experiment with pso-TFO-PEG5K (**Fig 3C**), except that the mobilities of all detected adducts was shifted accordingly to the extra molecular weight of PEG5K, indicating that the bulky PEG5K residue did not interfere with the efficiency of pso-dependent crosslinking in origami. Crosslinking of 1HP-pso-TFO complexes prepared by the one-pot method followed the same kinetics as crosslinking of 1HP origami saturated by pso-TFO (compare 1HP origami gels in Figs 3C and 3D). In all cases, the pso-TFO-dependent crosslinking of 1HP was highly specific as no significant amounts of adducts of sizes bigger than the expected bis-adduct were detectable on the PAGE gels.

In origami containing adjacent TFO-binding hairpins, a single staple can participate in the formation of two hairpins – one hairpin at the 5′ end (formed by the 4-nt staple extension) and another one at the 3′ end (formed by the 32-nt extension). We therefore asked if “super-staples” can form upon crosslinking of adjacent hairpins. Thus, we purified origami in which we added 1 (2HP) or 2 (3HP) additional hairpins adjacent to the hairpin formed by staple 0 and staple 1 (**Fig S4** and **Fig 3A**). This time experiments were performed on origami prepared using our one-pot assembly approach (**Fig 3D**). It was observed that, after irradiation for 1 and 9 seconds, both the 2HP and 3HP origami formed crosslinked species that migrated much slower than those observed for 1HP. This is consistent with formation of a three-staple adduct for 2HP, presumably mediated by two pso-TFOs, and a four-staple adduct for 3HP, presumably mediated by three pso-TFOs. Longer irradiation times did not significantly affect the pattern of crosslinking products, indicating that the formation of super-staples went to saturation (data not shown). We conclude that the targeting of proximal hairpins in origami leads to the formation of “super-staples” and that this site-specifically tethers the pso-TFO (and attached functionality) to precise locations on the origami. We also note that irradiation of the Cy5-labeled DNA constructs for 3 seconds did not cause significant changes in Cy5 fluorescence in species detectable by PAGE, whilst irradiation for 9 seconds resulted in only a small ~20%

decrease in Cy5 fluorescence (**Fig S6**). This indicates that the power density of 365 nm irradiation used by our mini-LED is mostly benign to fluorophores attached to origami.

Improving the structural integrity of functionalised origami

Since our crosslinking strategy leads to the formation of "super-staples" within HP-origami, we next asked if this increases the thermal stability of the functionalised nanostructures (**Fig 4**). We used AGE analysis to monitor origami denaturation at specific temperatures using the following as signals: (i) the release of the Cy5-labeled staple 1, which migrates below the 0.5 kb dsDNA marker; (ii) the decrease of the Cy5 signal in the origami; and (iii) the conversion of the origami into the faster migrating ssDNA scaffold. Where appropriate, AGE analysis was supported by TEM imaging of the heat-treated nanostructures.

We first determined the effect of a 50 °C temperature challenge on 258HP origami that had been irradiated for 10 seconds in the presence and absence of a pso-TFO carrying a PEG_4-NH_2 group (pso-TFO-PEG_4-NH_2). AGE analysis of the TFO-free origami revealed that the nanostructure underwent rapid unfolding between the 20- and 30-sec timepoints, with no intermediates detectable within the time resolution of this assay (**Fig 4A, top panel**). This agrees with previously reported studies that show that the melting of staples within origami occurs cooperatively.[49] TEM imaging also confirmed that after a 50-second incubation there were no intact origami remaining in the sample (**Fig 4C**). We next investigated if saturating and crosslinking the purified 258HP origami in the presence of a ~70-fold excess of pso-TFO over hairpins led to an enhancement in the stability of the complexes. Strikingly, we found that irradiated pso-TFO-loaded 258HP remained intact for at least 6250 seconds (~1.7 hours), consistent with at least a 250-fold increase in the lifetime (**Fig 4A, middle panel**). Finally, we asked if complexes prepared and crosslinked using our one-pot assembly method exhibited the same level of stabilisation. AGE analysis revealed that the structures appeared as stable as the TFO-saturated origami, and no unfolding products were again detectable for at least ~1.7 hours (**Fig 4A, bottom panel**). This was consistent with TEM imaging which showed that after incubation for 1250 seconds the complexes remained intact (**Fig 4D**).

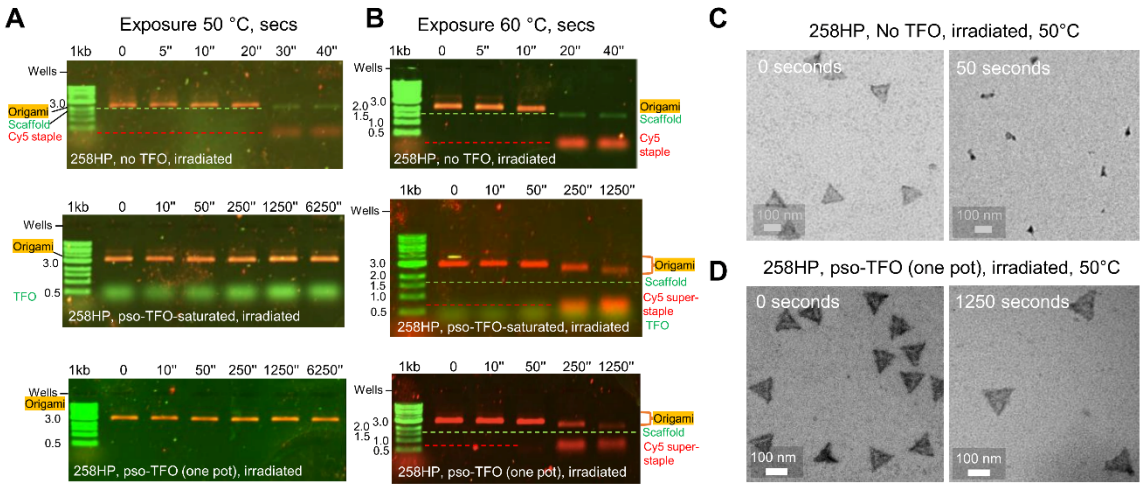

Figure 4. Heat challenge of 258HP origami subjected to pso-TFO driven crosslinking. (A and B) Experiments were undertaken on origami folded in the absence (top panel) or presence of pso-TFO-PEG_4-NH_2 under saturating (middle panel) or one-pot annealing (bottom panel) conditions. Origami containing pso-TFOs were subjected to irradiation at 365 nm for 10 seconds. Samples of 2 nM folded origami were then subjected to heat challenge at either 50 °C **(A)** or 60 °C **(B)** for the timepoints indicated. Samples were run on a 1% agarose gel in a pH 4.8 running buffer at room temperature. Bands for the origami and "super-staples" were visualised by scanning for Cy5-reporter sstaple fluorescence, whilst the scaffold strand, free TFO and dsDNA markers were visualised by scanning for ethidium bromide fluorescence; **(C)** Representative TEM images of 258HP origami prepared in the absence of TFO, irradiated and subjected to heat challenge for 0 and 50 seconds; **(D)** Representative TEM images of 258HP origami prepared in the presence of TFO, irradiated and subjected to heat challenge for 0 and 1250 seconds.

To probe the limits of pso-TFO-driven stabilization, we repeated the panel of thermal challenge experiments at a higher temperature of 60°C, using the same three types of irradiated origami. This time, AGE analysis showed that the TFO-free origami unfolded completely in 10-20 seconds, *i.e.,* at an expectedly faster rate than at 50 °C (**Fig 4B, top panel**). In contrast, the TFO-crosslinked origami remained intact for at least 50 seconds, irrespective of whether the complexes had been saturated with TFO or had been prepared by one-pot assembly. Further incubation at 60 °C caused partial unfolding of the crosslinked origami which was detected as (i) a ~3-fold and 8-fold reduction in fluorescence in the Cy5-labeled origami at 250 and 1250 seconds, respectively, and (ii) a progressive downward shift in the Cy5-labeled origami at 250 and 1250 seconds (**Fig 4B, middle and bottom panels**). Despite partial unfolding, the migration of both types of crosslinked origami never reached the level of the Cy5-free ssDNA scaffold, indicating that they might have retained some structural elements despite prolonged incubation at 60°C. In addition, a Cy5-labeled species appeared below the origami band which migrated between the 0.5 and 1 kb dsDNA markers. This species is likely to be similar in nature to the "super-staples" observed in the 2HP and 3HP origami crosslinking experiments (**Fig 3D**). Overall, these temperature challenge experiments indicate that pso-TFO mediated

crosslinking leads to a dramatic stabilization of the HP-origami and is not affected by the method of their assembly. These experiments also confirmed that irradiated origami undergo incomplete crosslinking, as the fully crosslinked super-staple (comprised of 258 hairpins) would be expected to migrate at the rate of the ssDNA scaffold (migrates at ~1.7 kb), or a heavier species.

We then asked if TFO-directed crosslinking improves the resistance of functionalised origami to DNA-processing enzymes. We chose phage T7 RNA polymerase (T7 RNAP) as a suitable test since it has been shown to induce disassembly of DNA nanostructures by promoter-independent transcription.[25] We reasoned that formation of the "super-staples" might provide “self-healing” properties to the origami and protect the structures from RNAP-dependent strand displacement. To test this, we first incubated purified TFO-free 258HP origami with a 2.5 uM T7 RNAP (500-fold molar excess), conditions that mimicked the estimated *in vivo* concentrations of commonly studied RNAPs.[50,51] The origami was incubated with RNAP at 37 °C for 30 minutes and then treated with proteinase K before analysing the samples by AGE (**Fig 5A, top panel**). Analysis showed that, in the absence of nucleotide triphosphates (NTPs), most of the origami became distorted, but not disassembled by RNAP, as evidenced by the appearance of a step/smear pattern from the origami band to the well in the gel and by the absence of the released Cy5-labelled reporter staple (compare lanes 2 and 3). In contrast, incubation with RNAP in the presence of 0.5 mM NTPs resulted in complete destruction of the TFO-free origami, as seen from the full transition of the Cy5 signal from the origami band into the released Cy5-staple (lane 4). In addition, a strong smear detectable by ethidium bromide, migrating between the Cy5-labelled staple and the 0.5 kb dsDNA marker, appeared after incubation. Further incubation with RNase removed the smear, indicating that it represented the RNA non-specifically transcribed by RNAP from the nanostructures (lane 5). We conclude that TFO-free 258HP origami are bound by RNAP in the absence of NTPs and are disassembled under conditions permitting transcription.[25]

We next investigated if TFO-crosslinked origami became resistant to RNAP transcription (**Fig 5A**, **middle panel**). We found that, in the absence of NTPs, the crosslinked complexes appeared intact after the RNAP challenge, indicating that, under NTP-free conditions, TFO loading and/or crosslinking reduces the affinity of RNAP for the origami (compare lanes 1 and 2). Most importantly, in the presence of NTPs, the crosslinked complexes appeared resistant to RNAP disassembly (lane 4). Interestingly, the RNA smear was still detectable after the transcription challenge, indicating that RNAP could still transcribe the crosslinked origami, but presumably could not displace the “super-staples” from the scaffold (lane 3). We thus investigated whether we could eliminate this residual transcription activity by attaching the

bulky PEG20K to the 5′ end of the TFO (**Fig 5A, bottom panel**). We found that the crosslinked 258HP-TFO-PEG20K complexes were indistinguishable from the PEG-free 258HP-TFO complexes, *i.e.,* they remained intact after transcription and still supported RNAP transcriptional activity. This finding was confirmed by TEM imaging which showed mostly intact 258HP-pso-TFO-PEG20K complexes after transcription, with minor damage in the triangle centres where the 3 central staples lacked hairpins due to design constraints (see Supplementary Table 1) and at the sector joints (perhaps due to the low density of TFO-binding hairpins at these positions) (**Fig 5B**). We conclude that internal crosslinking by pso-TFOs and their conjugates protects HP origami from destruction by transcribing RNAP.

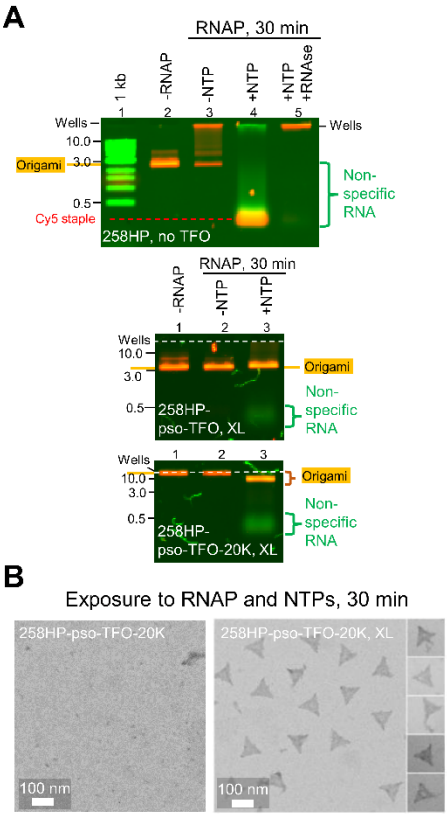

Figure 5. RNAP challenge of 258HP origami subjected to pso-TFO-driven crosslinking. (A) Experiments were undertaken on origami folded in the absence (top panel) or presence of a pso-TFO (middle) or its PEG20K conjugate (bottom panel). These were prepared under one-pot annealing conditions and the origami containing pso-TFOs were subjected to irradiation at 365 nm for 10 seconds. Samples of 2-5 nM folded origami were then incubated with 2.5 μM T7 RNAP in the presence or absence of 1 mM NTPs at 37 °C for 30 minutes and then subjected to proteinase K treatment for 15 minutes to degrade the protein. Additional samples that were subjected to RNase A treatment before proteinase K digestion were also prepared. Samples were run on a 1% agarose gel in a pH 4.8 running buffer at room temperature. Bands for the origami and the Cy5-labelled staple 1 were visualised by scanning for Cy5 fluorescence, whilst RNA transcripts and dsDNA markers were visualised by scanning for ethidium bromide fluorescence; **(B)** Representative TEM images of non-irradiated (left image) and irradiated (right image) 258HP-pso-TFO-PEG20K origami that had been subjected to RNAP challenge in the presence of NTPs.

DISCUSSION

Here we have developed an approach that extends triplex-directed functionalization and crosslinking from DNA tiles to DNA origami.[34,37,38] We have shown that TFOs can target hairpin duplexes introduced at single, multiple, or almost all of the nick sites between staples within a prototypical DNA origami structure, with ~90% loading efficiency. Functionalization of origami with amine and biotin groups was achieved by attaching cargo to the 3′ of the TFO and was effective even for bulky PEG5K/20K groups. Introduction of the groups was possible during or after assembly, without disruption to the underlying origami scaffold. Most importantly, we show that the TFO (and attached groups) can be covalently crosslinked to the origami with >80% crosslinking efficiency using psoralen-5′-labelled TFOs. We show that 60-80% of the adducts formed by psoralen are bis-adducts that tie the TFO to both staple strands of the assembled hairpins, and the yield of the crosslinked products was consistent with previous studies.[52] Directing crosslinking reactions between proximal hairpins led to the generation of "super-staples" that prevents the stochastic dissociation of the staple (and attached TFO conjugate) from the structure. Since psoralen crosslinking utilises mild UVA light, we also demonstrated that efficient crosslinking was possible using fast irradiation times (<10 secs) and a simple narrow-band LED as a light source. Compared to other crosslinking approaches, our approach is scalable, site-specific[20] and less damaging to the structural integrity of the origami scaffold,[31] as well as to functionalities introduced into the structure (*e.g.,* fluorophores). Further increase in crosslinking efficiency might also be possible using TFOs containing multiple psoralen molecules (*e.g.* "triplex staples"[53]) or using TFOs that contain stabilizing nucleotide analogues.[54,55]

We also demonstrated that, through the appropriate positioning of hairpins, such TFO-functionalised, crosslinked structures become less susceptible to thermal denaturation and completely resistant to disassembly by concentrated phage T7 RNAP. Our RNAP sensitivity assay was inspired by the motivation to employ DNA origami as platforms for *in vitro* and *in vivo* single-molecule analyses of transcription initiation. We anticipated that un-crosslinked origami would be highly vulnerable to RNAPs, since origami, by definition, have numerous nicks and often have ssDNA modules, whereas RNAPs are known to non-specifically initiate from nicks[56,57,58,59] and ssDNA.[60] Sensitivity of nanostructures to viral RNAPs has been recently documented.[25] We showed that TFO-driven crosslinking protected origamis from destruction by the transcribing T7 RNAP, consistent with the notion that the super-staples formed by crosslinking could not be irreversibly displaced by the transcribing enzyme. The finding that the crosslinked origami were still transcribed by RNAP showed that the nanostructure remained accessible to RNAP despite the presence of TFO, or the

functionalization of the TFO 3′ end with the bulky PEG20K group. Optimization of the hairpin placement and/or the TFO functionalities will be needed to fully control non-specific origami binding by RNAP and other DNA-processing enzymes. Overall, the RNAP sensitivity assay offers more nuanced metrics of origami functionality in biological media compared to nuclease sensitivity assays,[24] since it provides three separate read-outs – non-specific RNAP binding/distortion of origami, staple displacement, and RNA production.

Recently, triplex motifs have been used as secondary structural elements capable of compacting dsDNA into various new DNA origami architectures.[34,61,62] Such structures are assembled from designer scaffolds containing multiple distinct polypurine-polypyrimidine TFO target sequences folded by triplex-mediated crossover strand exchange. Our functionalization strategy could extend this design process, *e.g.,* by attaching psoralen and other cargo to the crossover TFOs. The combination of such triplex technologies will result in a new generation of functionalized origami nanostructures that exhibit enhanced configurability and stability over those obtained with their duplex-only counterparts. This is likely to have most benefit with origami designed for use in biomedical science, where maintaining the structural integrity and function of the origami is paramount.

Acknowledgements

We thank Ian Eperon and Glen Burley for advice on experimental design, Paul Rothemund and Shawn Douglas for advice on DNA origami design, and Olga Makarova for advice on DNA origami purification. A.R. thanks the University of Leicester and the BBSRC (BB/L021730/1) for support.

Conflict of interest statement

Rafael del Villar Guerra is currently an employee of AstraZeneca and may own stock or stock options.

REFERENCES

(1) Seeman, N. C.; Sleiman, H. F. DNA Nanotechnology. *Nat. Rev. Mater.* **2017**, *3* (1), 17068. https://doi.org/10.1038/natrevmats.2017.68.
(2) Dey, S.; Fan, C.; Gothelf, K. V.; Li, J.; Lin, C.; Liu, L.; Liu, N.; Nijenhuis, M. A. D.; Saccà, B.; Simmel, F. C.; Yan, H.; Zhan, P. DNA Origami. *Nat. Rev. Methods Primer* **2021**, *1* (1), 13. https://doi.org/10.1038/s43586-020-00009-8.
(3) Rothemund, P. W. K. Folding DNA to Create Nanoscale Shapes and Patterns. *Nature* **2006**, *440* (7082), 297–302. https://doi.org/10.1038/nature04586.
(4) Douglas, S. M.; Marblestone, A. H.; Teerapittayanon, S.; Vazquez, A.; Church, G. M.; Shih, W. M. Rapid Prototyping of 3D DNA-Origami Shapes with CaDNAno. *Nucleic Acids Res.* **2009**, *37* (15), 5001–5006. https://doi.org/10.1093/nar/gkp436.
(5) Knappe, G. A.; Wamhoff, E.-C.; Bathe, M. Functionalizing DNA Origami to Investigate and Interact with Biological Systems. *Nat. Rev. Mater.* **2022**, *8* (2), 123–138. https://doi.org/10.1038/s41578-022-00517-x.
(6) Oktay, E.; Alem, F.; Hernandez, K.; Girgis, M.; Green, C.; Mathur, D.; Medintz, I. L.; Narayanan, A.; Veneziano, R. DNA Origami Presenting the Receptor Binding Domain of SARS-CoV-2 Elicit Robust Protective Immune Response. *Commun. Biol.* **2023**, *6* (1), 308. https://doi.org/10.1038/s42003-023-04689-2.
(7) Ke, G.; Liu, M.; Jiang, S.; Qi, X.; Yang, Y. R.; Wootten, S.; Zhang, F.; Zhu, Z.; Liu, Y.; Yang, C. J.; Yan, H. Directional Regulation of Enzyme Pathways through the Control of Substrate Channeling on a DNA Origami Scaffold. *Angew. Chem. Int. Ed.* **2016**, *55* (26), 7483–7486. https://doi.org/10.1002/anie.201603183.
(8) Selnihhin, D.; Sparvath, S. M.; Preus, S.; Birkedal, V.; Andersen, E. S. Multifluorophore DNA Origami Beacon as a Biosensing Platform. *ACS Nano* **2018**, *12* (6), 5699–5708. https://doi.org/10.1021/acsnano.8b01510.
(9) Ramezani, H.; Dietz, H. Building Machines with DNA Molecules. *Nat. Rev. Genet.* **2020**, *21* (1), 5–26. https://doi.org/10.1038/s41576-019-0175-6.
(10) Zhang, Q.; Jiang, Q.; Li, N.; Dai, L.; Liu, Q.; Song, L.; Wang, J.; Li, Y.; Tian, J.; Ding, B.; Du, Y. DNA Origami as an *In Vivo* Drug Delivery Vehicle for Cancer Therapy. *ACS Nano* **2014**, *8* (7), 6633–6643. https://doi.org/10.1021/nn502058j.
(11) Steinhauer, C.; Jungmann, R.; Sobey, T.; Simmel, F.; Tinnefeld, P. DNA Origami as a Nanoscopic Ruler for Super-Resolution Microscopy. *Angew. Chem. Int. Ed.* **2009**, *48* (47), 8870–8873. https://doi.org/10.1002/anie.200903308.
(12) Martin, T. G.; Bharat, T. A. M.; Joerger, A. C.; Bai, X.; Praetorius, F.; Fersht, A. R.; Dietz, H.; Scheres, S. H. W. Design of a Molecular Support for Cryo-EM Structure

Determination. *Proc. Natl. Acad. Sci.* **2016**, *113* (47). https://doi.org/10.1073/pnas.1612720113.
(13) Kramm, K.; Schröder, T.; Gouge, J.; Vera, A. M.; Gupta, K.; Heiss, F. B.; Liedl, T.; Engel, C.; Berger, I.; Vannini, A.; Tinnefeld, P.; Grohmann, D. DNA Origami-Based Single-Molecule Force Spectroscopy Elucidates RNA Polymerase III Pre-Initiation Complex Stability. *Nat. Commun.* **2020**, *11* (1), 2828. https://doi.org/10.1038/s41467-020-16702-x.
(14) Shen, W.; Zhong, H.; Neff, D.; Norton, M. L. NTA Directed Protein Nanopatterning on DNA Origami Nanoconstructs. *J. Am. Chem. Soc.* **2009**, *131* (19), 6660–6661. https://doi.org/10.1021/ja901407j.
(15) Voigt, N. V.; Tørring, T.; Rotaru, A.; Jacobsen, M. F.; Ravnsbæk, J. B.; Subramani, R.; Mamdouh, W.; Kjems, J.; Mokhir, A.; Besenbacher, F.; Gothelf, K. V. Single-Molecule Chemical Reactions on DNA Origami. *Nat. Nanotechnol.* **2010**, *5* (3), 200–203. https://doi.org/10.1038/nnano.2010.5.
(16) Kuzuya, A.; Kimura, M.; Numajiri, K.; Koshi, N.; Ohnishi, T.; Okada, F.; Komiyama, M. Precisely Programmed and Robust 2D Streptavidin Nanoarrays by Using Periodical Nanometer-Scale Wells Embedded in DNA Origami Assembly. *ChemBioChem* **2009**, *10* (11), 1811–1815. https://doi.org/10.1002/cbic.200900229.
(17) Chhabra, R.; Sharma, J.; Ke, Y.; Liu, Y.; Rinker, S.; Lindsay, S.; Yan, H. Spatially Addressable Multiprotein Nanoarrays Templated by Aptamer-Tagged DNA Nanoarchitectures. *J. Am. Chem. Soc.* **2007**, *129* (34), 10304–10305. https://doi.org/10.1021/ja072410u.
(18) Nakata, E.; Liew, F. F.; Uwatoko, C.; Kiyonaka, S.; Mori, Y.; Katsuda, Y.; Endo, M.; Sugiyama, H.; Morii, T. Zinc-Finger Proteins for Site-Specific Protein Positioning on DNA-Origami Structures. *Angew. Chem. Int. Ed.* **2012**, *51* (10), 2421–2424. https://doi.org/10.1002/anie.201108199.
(19) Linko, V.; Keller, A. Stability of DNA Origami Nanostructures in Physiological Media: The Role of Molecular Interactions. *Small* **2023**, 2301935. https://doi.org/10.1002/smll.202301935.
(20) Rajendran, A.; Endo, M.; Katsuda, Y.; Hidaka, K.; Sugiyama, H. Photo-Cross-Linking-Assisted Thermal Stability of DNA Origami Structures and Its Application for Higher-Temperature Self-Assembly. *J. Am. Chem. Soc.* **2011**, *133* (37), 14488–14491. https://doi.org/10.1021/ja204546h.
(21) Ramakrishnan, S.; Krainer, G.; Grundmeier, G.; Schlierf, M.; Keller, A. Structural Stability of DNA Origami Nanostructures in the Presence of Chaotropic Agents. *Nanoscale* **2016**, *8* (19), 10398–10405. https://doi.org/10.1039/C6NR00835F.
(22) Martin, T. G.; Dietz, H. Magnesium-Free Self-Assembly of Multi-Layer DNA Objects. *Nat. Commun.* **2012**, *3* (1), 1103. https://doi.org/10.1038/ncomms2095.
(23) Kim, H.; Surwade, S. P.; Powell, A.; O'Donnell, C.; Liu, H. Stability of DNA Origami Nanostructure under Diverse Chemical Environments. *Chem. Mater.* **2014**, *26* (18), 5265–5273. https://doi.org/10.1021/cm5019663.
(24) Chandrasekaran, A. R. Nuclease Resistance of DNA Nanostructures. *Nat. Rev. Chem.* **2021**, *5* (4), 225–239. https://doi.org/10.1038/s41570-021-00251-y.
(25) Schaffter, S. W.; Green, L. N.; Schneider, J.; Subramanian, H. K. K.; Schulman, R.; Franco, E. T7 RNA Polymerase Non-Specifically Transcribes and Induces Disassembly of DNA Nanostructures. *Nucleic Acids Res.* **2018**, *46* (10), 5332–5343. https://doi.org/10.1093/nar/gky283.
(26) Rajendran, A.; Krishnamurthy, K.; Giridasappa, A.; Nakata, E.; Morii, T. Stabilization and Structural Changes of 2D DNA Origami by Enzymatic Ligation. *Nucleic Acids Res.* **2021**, *49* (14), 7884–7900. https://doi.org/10.1093/nar/gkab611.
(27) Weizenmann, N.; Scheidgen-Kleyboldt, G.; Ye, J.; Krause, C. B.; Kauert, D.; Helmi, S.; Rouillon, C.; Seidel, R. Chemical Ligation of an Entire DNA Origami Nanostructure. *Nanoscale* **2021**, *13* (41), 17556–17565. https://doi.org/10.1039/D1NR04225D.
(28) Cassinelli, V.; Oberleitner, B.; Sobotta, J.; Nickels, P.; Grossi, G.; Kempter, S.; Frischmuth, T.; Liedl, T.; Manetto, A. One-Step Formation of "Chain-Armor"-Stabilized

DNA Nanostructures. *Angew. Chem. Int. Ed.* **2015**, *54* (27), 7795–7798. https://doi.org/10.1002/anie.201500561.
(29) Gerling, T.; Kube, M.; Kick, B.; Dietz, H. Sequence-Programmable Covalent Bonding of Designed DNA Assemblies. *Sci. Adv.* **2018**, *4* (8), eaau1157. https://doi.org/10.1126/sciadv.aau1157.
(30) Engelhardt, F. A. S.; Praetorius, F.; Wachauf, C. H.; Brüggenthies, G.; Kohler, F.; Kick, B.; Kadletz, K. L.; Pham, P. N.; Behler, K. L.; Gerling, T.; Dietz, H. Custom-Size, Functional, and Durable DNA Origami with Design-Specific Scaffolds. *ACS Nano* **2019**, *13* (5), 5015–5027. https://doi.org/10.1021/acsnano.9b01025.
(31) Chen, H.; Li, R.; Li, S.; Andréasson, J.; Choi, J. H. Conformational Effects of UV Light on DNA Origami. *J. Am. Chem. Soc.* **2017**, *139* (4), 1380–1383. https://doi.org/10.1021/jacs.6b10821.
(32) Moser, H. E.; Dervan, P. B. Sequence-Specific Cleavage of Double Helical DNA by Triple Helix Formation. *Science* **1987**, *238* (4827), 645–650. https://doi.org/10.1126/science.3118463.
(33) Dalla Pozza, M.; Abdullrahman, A.; Cardin, C. J.; Gasser, G.; Hall, J. P. Three's a Crowd – Stabilisation, Structure, and Applications of DNA Triplexes. *Chem. Sci.* **2022**, *13* (35), 10193–10215. https://doi.org/10.1039/D2SC01793H.
(34) Chandrasekaran, A. R.; Rusling, D. A. Triplex-Forming Oligonucleotides: A Third Strand for DNA Nanotechnology. *Nucleic Acids Res.* **2018**, *46* (3), 1021–1037. https://doi.org/10.1093/nar/gkx1230.
(35) Hu, Y.; Cecconello, A.; Idili, A.; Ricci, F.; Willner, I. Triplex DNA Nanostructures: From Basic Properties to Applications. *Angew. Chem. Int. Ed.* **2017**, *56* (48), 15210–15233. https://doi.org/10.1002/anie.201701868.
(36) Rusling, D. A.; Nandhakumar, I. S.; Brown, T.; Fox, K. R. Triplex-Directed Recognition of a DNA Nanostructure Assembled by Crossover Strand Exchange. *ACS Nano* **2012**, *6* (4), 3604–3613. https://doi.org/10.1021/nn300718z.
(37) Rusling, D. A.; Chandrasekaran, A. R.; Ohayon, Y. P.; Brown, T.; Fox, K. R.; Sha, R.; Mao, C.; Seeman, N. C. Functionalizing Designer DNA Crystals with a Triple-Helical Veneer. *Angew. Chem. Int. Ed.* **2014**, *53* (15), 3979–3982. https://doi.org/10.1002/anie.201309914.
(38) Zhao, Y.; Chandrasekaran, A. R.; Rusling, D. A.; Woloszyn, K.; Hao, Y.; Hernandez, C.; Vecchioni, S.; Ohayon, Y. P.; Mao, C.; Seeman, N. C.; Sha, R. The Formation and Displacement of Ordered DNA Triplexes in Self-Assembled Three-Dimensional DNA Crystals. *J. Am. Chem. Soc.* **2023**, *145* (6), 3599–3605. https://doi.org/10.1021/jacs.2c12667.
(39) Takasugi, M.; Guendouz, A.; Chassignol, M.; Decout, J. L.; Lhomme, J.; Thuong, N. T.; Hélène, C. Sequence-Specific Photo-Induced Cross-Linking of the Two Strands of Double-Helical DNA by a Psoralen Covalently Linked to a Triple Helix-Forming Oligonucleotide. *Proc. Natl. Acad. Sci.* **1991**, *88* (13), 5602–5606. https://doi.org/10.1073/pnas.88.13.5602.
(40) Abdallah, H. O.; Ohayon, Y. P.; Chandrasekaran, A. R.; Sha, R.; Fox, K. R.; Brown, T.; Rusling, D. A.; Mao, C.; Seeman, N. C. Stabilisation of Self-Assembled DNA Crystals by Triplex-Directed Photo-Cross-Linking. *Chem. Commun.* **2016**, *52* (51), 8014–8017. https://doi.org/10.1039/C6CC03695C.
(41) Rusling, D. A.; Nandhakumar, I. S.; Brown, T.; Fox, K. R. Triplex-Directed Covalent Cross-Linking of a DNA Nanostructure. *Chem. Commun.* **2012**, *48* (77), 9592. https://doi.org/10.1039/c2cc35407a.
(42) Douglas, S. M.; Dietz, H.; Liedl, T.; Högberg, B.; Graf, F.; Shih, W. M. Self-Assembly of DNA into Nanoscale Three-Dimensional Shapes. *Nature* **2009**, *459* (7245), 414–418. https://doi.org/10.1038/nature08016.
(43) Lin, C.; Perrault, S. D.; Kwak, M.; Graf, F.; Shih, W. M. Purification of DNA-Origami Nanostructures by Rate-Zonal Centrifugation. *Nucleic Acids Res.* **2013**, *41* (2), e40–e40. https://doi.org/10.1093/nar/gks1070.

(44) Suma, A.; Stopar, A.; Nicholson, A. W.; Castronovo, M.; Carnevale, V. Global and Local Mechanical Properties Control Endonuclease Reactivity of a DNA Origami Nanostructure. *Nucleic Acids Res.* **2020**, *48* (9), 4672–4680. https://doi.org/10.1093/nar/gkaa080.
(45) Kim, H.; Surwade, S. P.; Powell, A.; O'Donnell, C.; Liu, H. Stability of DNA Origami Nanostructure under Diverse Chemical Environments. *Chem. Mater.* **2014**, *26* (18), 5265–5273. https://doi.org/10.1021/cm5019663.
(46) Zhang, Z.; Park, S.; Pertsinidis, A.; Revyakin, A. Cloud-Point PEG Glass Surfaces for Imaging of Immobilized Single Molecules by Total-Internal-Reflection Microscopy. *BIO-Protoc.* **2016**, *6* (7). https://doi.org/10.21769/BioProtoc.1784.
(47) Visnapuu, M.-L.; Duzdevich, D.; Greene, E. C. The Importance of Surfaces in Single-Molecule Bioscience. *Mol. Biosyst.* **2008**, *4* (5), 394. https://doi.org/10.1039/b800444g.
(48) Katz, B. A. Binding of Biotin to Streptavidin Stabilizes Intersubunit Salt Bridges between Asp61 and His87 at Low PH. *J. Mol. Biol.* **1997**, *274* (5), 776–800. https://doi.org/10.1006/jmbi.1997.1444.
(49) Wei, X.; Nangreave, J.; Jiang, S.; Yan, H.; Liu, Y. Mapping the Thermal Behavior of DNA Origami Nanostructures. *J. Am. Chem. Soc.* **2013**, *135* (16), 6165–6176. https://doi.org/10.1021/ja4000728.
(50) Patrick, M.; Dennis, P. P.; Ehrenberg, M.; Bremer, H. Free RNA Polymerase in Escherichia Coli. *Biochimie* **2015**, *119*, 80–91. https://doi.org/10.1016/j.biochi.2015.10.015.
(51) Jackson, D. A.; Pombo, A.; Iborra, F. The Balance Sheet for Transcription: An Analysis of Nuclear RNA Metabolism in Mammalian Cells. *FASEB J. Off. Publ. Fed. Am. Soc. Exp. Biol.* **2000**, *14* (2), 242–254.
(52) Smith, S. I.; Brodbelt, J. S. Rapid Characterization of Cross-Links, Mono-Adducts, and Non-Covalent Binding of Psoralens to Deoxyoligonucleotides by LC-UV/ESI-MS and IRMPD Mass Spectrometry. *The Analyst* **2010**, *135* (5), 943. https://doi.org/10.1039/b924023c.
(53) Li, H.; Broughton-Head, V. J.; Peng, G.; Powers, V. E. C.; Ovens, M. J.; Fox, K. R.; Brown, T. Triplex Staples: DNA Double-Strand Cross-Linking at Internal and Terminal Sites Using Psoralen-Containing Triplex-Forming Oligonucleotides. *Bioconjug. Chem.* **2006**, *17* (6), 1561–1567. https://doi.org/10.1021/bc0601875.
(54) Rusling, D. A. Triplex-Forming Properties and Enzymatic Incorporation of a Base-Modified Nucleotide Capable of Duplex DNA Recognition at Neutral PH. *Nucleic Acids Res.* **2021**, *49* (13), 7256–7266. https://doi.org/10.1093/nar/gkab572.
(55) Walsh, S.; El-Sagheer, A. H.; Brown, T. Fluorogenic Thiazole Orange TOTFO Probes Stabilise Parallel DNA Triplexes at PH 7 and Above. *Chem. Sci.* **2018**, *9* (39), 7681–7687. https://doi.org/10.1039/C8SC02418A.
(56) Dynan, W. S.; Burgess, R. R. In Vitro Transcription by Wheat Germ RNA Polymerase II. Initiation of RNA Synthesis on Relaxed, Closed Circular Template. *J. Biol. Chem.* **1981**, *256* (11), 5866–5873. https://doi.org/10.1016/S0021-9258(19)69288-4.
(57) Dreyer, C.; Hausen, P. On the Initiation of Mammalian RNA Polymerase at Single-Strand Breaks in DNA. *Eur. J. Biochem.* **1976**, *70* (1), 63–74. https://doi.org/10.1111/j.1432-1033.1976.tb10956.x.
(58) Chandler, D. W.; Gralla, J. The Interaction of RNA Polymerase II with Non-Promoter DNA Sites. *Nucleic Acids Res.* **1981**, *9* (22), 6031–6046. https://doi.org/10.1093/nar/9.22.6031.
(59) Vogt, V. Breaks in DNA Stimulate Transcription by Core RNA Polymerase. *Nature* **1969**, *223* (5208), 854–855. https://doi.org/10.1038/223854a0.
(60) Ishihama, A.; Murakami, S.; Fukuda, R.; Matsukage, A.; Kameyama, T. The Nature of Initiation Sites on DNA for the Core RNA Polymerase. *Mol. Gen. Genet. MGG* **1971**, *111* (1), 66–76. https://doi.org/10.1007/BF00286555.
(61) Sachenbacher, K.; Khoshouei, A.; Honemann, M. N.; Engelen, W.; Feigl, E.; Dietz, H. Triple-Stranded DNA As a Structural Element in DNA Origami. *ACS Nano* **2023**, *17* (10), 9014–9024. https://doi.org/10.1021/acsnano.2c11402.

(62) Ng, C.; Samanta, A.; Mandrup, O. A.; Tsang, E.; Youssef, S.; Klausen, L. H.; Dong, M.; Nijenhuis, M. A. D.; Gothelf, K. V. Folding Double-Stranded DNA into Designed Shapes with Triplex-Forming Oligonucleotides. *Adv. Mater.* **2023**, 2302497. https://doi.org/10.1002/adma.202302497.